AN EXPERIMENTAL BICONVEX LIQUID-FILLED ACOUSTIC LENS

by

Jackie Lee Roudebush

United States Naval Postgraduate School

THESIS

AN EXPERIMENTAL BICONVEX
LIQUID-FILLED ACOUSTIC LENS

by

Jackie Lee Roudebush

June 1969

An Experimental Biconvex Liquid-filled Acoustic Lens

by

Jackie Lee Roudebush
Lieutenant Commander, United States Navy
B. S., Purdue University, 1960

Submitted in partial fulfillment of the
requirements for the degree of

ELECTRICAL ENGINEER

from the

NAVAL POSTGRADUATE SCHOOL
June 1969

ABSTRACT

An experimental study has been made of the properties of a biconvex liquid-filled acoustic lens formed by pressurizing a refracting fluid between two deformable diaphragms. Trichlorotrifluoroethane was used as the refracting liquid and stainless steel sheets 76 cm in diameter and 0.3 mm (0.012 inch) thick were used as the diaphragm material. Distortion of the spherical surfaces due to the weight of the liquid was negligible because of the tension developed by the internal hydrostatic pressure (1.4 atmospheres for focal length 1.2 meters). Acoustic diffraction patterns measured at f/4.0 in water at frequencies from 200 KHz to 500 KHz compare favorably with patterns computed numerically. Multiple focal points were found and can be associated with multiple internal reflections.

TABLE OF CONTENTS

I.	INTRODUCTION	5
II.	THEORY	7
	A. ASSUMPTIONS	7
	B. GEOMETRIC LOCATION OF FOCAL POINT	7
	C. DIFFRACTION PATTERN-NEGLECTING ABERRATIONS	10
	D. WAVEFRONT ABERRATIONS	12
	E. ADDITIONAL CONSIDERATIONS FOR AN ACTUAL LENS	17
	1. Fresnel Zones - Newton's Rings	17
	2. Multiple Reflections	23
III.	EXPERIMENT	24
	A. MECHANICAL DESIGN	24
	B. REFRACTING FLUID	30
	C. COMPUTER SIMULATION	33
	D. TRANSDUCERS	36
	E. TEST CONDITIONS	36
	F. PROBLEMS ENCOUNTERED	37
IV.	TEST RESULTS	40
V.	CONCLUSIONS	50
	A. GENERAL	50
	B. LENS CONSTRUCTION	50
	C. MULTIPLE FOCAL POINTS	51
LIST OF REFERENCES		52

INITIAL DISTRIBUTION LIST 54

FORM DD 1473 55

I. INTRODUCTION

Theoretical and experimental investigations of the focusing properties of spherical and cylindrical liquid-filled acoustic lenses have been conducted in the past by Boyles [Refs. 1, 2, 3, and 4], Folds and Brown [Refs. 5 and 6], and Toulis [Ref. 18]. One attempt to investigate the properties of a biconvex lens is reported by Foss and Levine [Ref. 7].

A basic problem in the physical design of liquid-filled acoustic lenses is the mechanical strength required of the container. For good energy transmission characteristics the refracting fluid (with sound velocity different from water) must have a characteristic impedance (ρc) nearly equal to that of water. If the index of refraction is n for the fluid, then the density of the fluid must be n times the density of water. The container material should also be a good ρc match and as thin as possible in order to minimize reflection losses due to the shell. There are some materials available which fulfill the acoustic requirements for containers; however, the mechanical strength of most of these materials is not sufficient to support the weight of large volumes of fluid without deformation and distortion of the lens surface.

An acoustic lens has a potential advantage over mirrors in acoustic imaging systems in that a lens eliminates the aperture blocking by the receiving system. And, in particular, a biconvex lens possesses some inherent advantages over the spherical lens when

large numerical apertures are desired. Among these advantages are:

1. A biconvex lens requires less fluid than a spherical lens with the same aperture. Since the refracting fluid is expensive, the biconvex lens is cheaper to build.

2. The radius of curvature of the lens and focal surfaces is larger for a biconvex lens than for a spherical lens.

3. The biconvex form can be generated simply by pressurizing the fluid between two deformable diaphragms.

Since there was little information available on the properties of a large biconvex liquid-filled acoustic lens and in view of the advantages to be gained by using such a lens, further investigation was undertaken.

II. THEORY

A. ASSUMPTIONS

The diffraction pattern of a point source is of primary concern in this analysis. In order to develop the theoretical properties of a liquid-filled acoustic lens the following assumptions are made:

1. Single-frequency, continuous-signal point source;

2. The lens and surrounding region of interest consist of isotropic, lossless fluids which differ only in index of refraction;

3. Rays are normal to pressure wavefronts;

4. Each element of a wavefront travels along its corresponding ray with a velocity equal to that of the speed of sound in the medium in question (except in the vicinity of the focus). Acoustic paths along the rays from source to wavefront are equal in length.

B. GEOMETRIC LOCATION OF FOCAL POINT

Figure 1 shows one ray from an object point at infinity entering the left surface of a simple thick lens, passing through the lens, and then intersecting the axis at the second focal point F'. First-order approximation gives

$$\frac{h}{s'_1} = \frac{h'}{-s'_2} \tag{1}$$

$$\frac{h}{f} = \frac{h'}{s'_2} \tag{2}$$

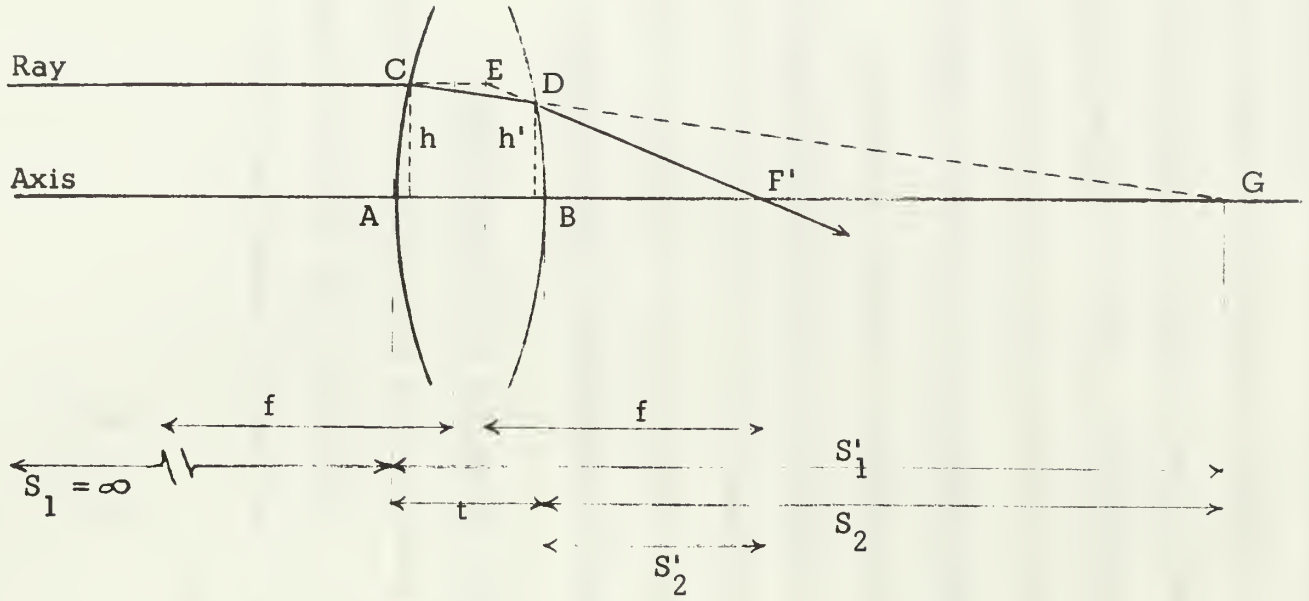

FIGURE 1

(Object distances (s) are positive when the object is to the left of the vertex. Image distances (s') are positive when the image lies to the right of the vertex.) Dividing (1) by (2) yields

$$f = s'_1 - \frac{s'_2}{s_2} \tag{3}$$

which is the accepted dimension called "focal length." However, s'_2 and the thickness (t) can be easily measured in an experiment; therefore, the following relations hold [Ref. 16].

$$\frac{1}{s_1} + \frac{n}{s'_1} = \frac{n-1}{R_1} \tag{4}$$

$$\frac{n}{s_2} + \frac{1}{s'_2} = \frac{1-n}{R_2} , \tag{5}$$

where

n = index of refraction of "lens liquid" relative to water. R_1 and R_2 are the radii of curvature of the left and right lens surfaces, respectively. Radius of curvature (R) is positive when the center of curvature lies to the right of the vertex. Inspection of Figure 1 shows that the distance s_2 is given by

$$s_2 = t - s'_1 \tag{6}$$

Letting s_1 go to infinity, as indicated in Figure 1, allows (4) to be written as

$$s'_1 = \frac{nR_1}{n-1} \tag{7}$$

Therefore,

$$s_2 = \frac{(n-1)t - nR_1}{n-1} \tag{7}$$

and substituting this into (5) yields,

$$s'_2 = - \frac{(n-1)\,[(n-1)t - nR_1] + n(n-1)R_2}{R_2[(n-1)r - nR_1]} \tag{8}$$

Actually, the value $s'_2 + t/2$ was measured in the experiment so that the theoretical location of the "paraxial focal point" must include the extra factor $t/2$.

C. DIFFRACTION PATTERN - NEGLECTING ABERRATIONS

It can be shown [Ref. 13] that a spherical wavefront emerging from a circular exit pupil of diameter D and converging to the geometrical image point (for an object at infinity the image point is the focal point determined by B above) produces a normalized diffraction pattern with intensity (I) in the plane normal to the axis through the geometrical image point given by

$$I = \left[\frac{2J_1(x)}{x}\right]^2 \tag{9}$$

where

J_1 is the Bessel function of order 1

$x = \left(\frac{2\pi r}{R}\right) \frac{\lambda}{D}$

R = distance from image point to the right vertex of lens

r = distance off-axis in the plane normal to the axis through the image point.

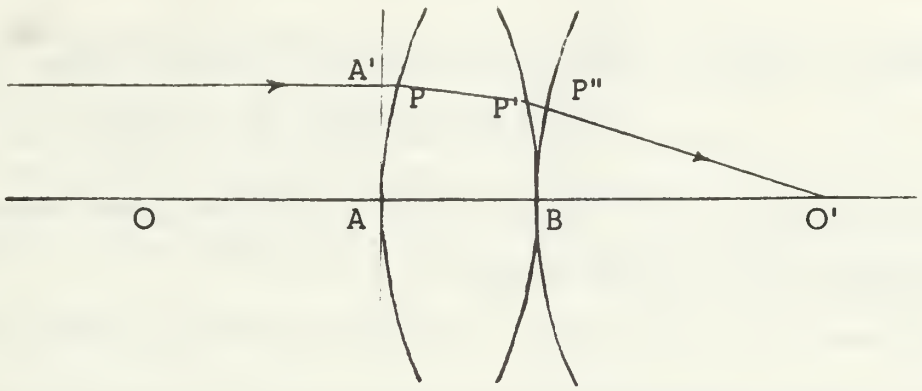

FIGURE 2

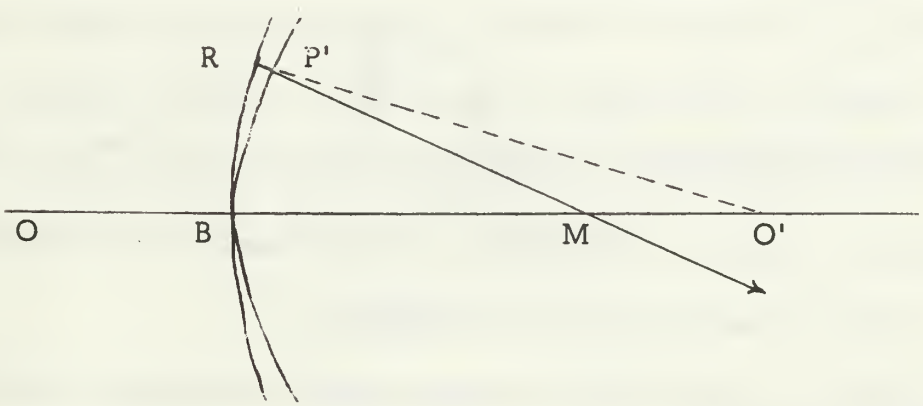

FIGURE 3

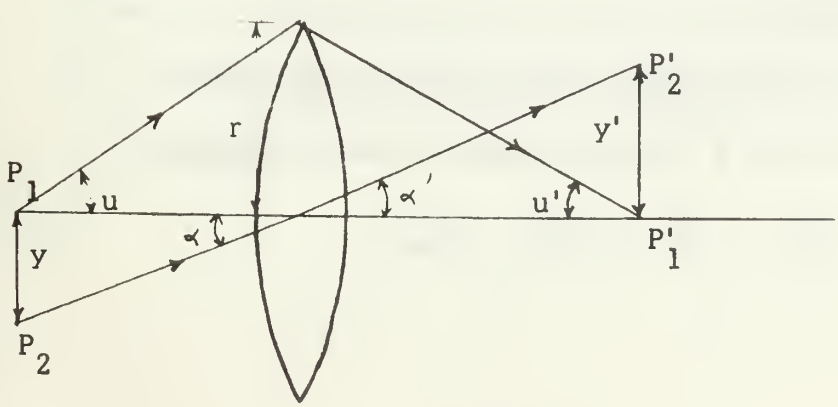

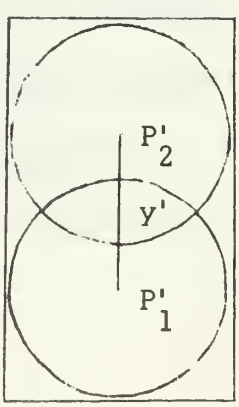

FIGURE 4

The first minimum of this function occurs at

$$r = (.61R)\frac{\lambda}{D} \tag{10}$$

Other minima occur when the numerical factor has values 1.12, 1.62, 2.12,...., and maxima occur for values of 0, 0.82, 1.33, 1.85,.... In addition, relative to the central maximum, the next three maxima have intensities of 0.017, 0.004, 0.0016.

D. WAVEFRONT ABERRATIONS

Figure 2 shows a ray entering the lens at P, exiting the lens at P' and passing through O'. If the ray PP'O' is considered to be limitingly close to the axis OO', then O' is the paraxial focal point determined in B. Under this assumption, O' becomes the center of curvature of the element of the wavefront on the axis and the emergent wavefront will be a portion of a sphere. Investigation of this element of the wavefront leads to the diffraction pattern discussed in C.

However, rays at finite distances from the axis do not intersect the axis at O'. Such rays intersect the axis to the left or right of O' depending on the shape of the lens face and the value of the index of refraction of the lens fluid.

If the physical length is denoted by a bar over the letters describing the ray in Figure 2, the assumptions made in A require

$$\overline{A'P} + n\,\overline{PP'} + \overline{P'P''} = n\,\overline{AB} \tag{11}$$

The most common occurrence is illustrated in Figure 3 where the actual wavefront lies "in front of" the sphere with center at O'. In fact, the distance by which the actual wavefront leads the sphere increases with increasing incident ray distance from the axis.

Since the emerging wavefront is not spherical, the intensity at the center of the diffraction pattern is decreased and the outer parts of the pattern become more intense. Figure 4 [Ref. 16] shows the diffraction pattern of two point sources greatly exaggerated.

According to the Rayleigh criterion, the linear distance between two "just resolvable" equally intense point sources is

$$y = \frac{.61}{\sin u} \tag{12}$$

when the intensity is given by equation (9). The minimum linear distance between the centers of the images is

$$y' = \frac{.61}{\sin u'} \tag{13}$$

It is apparent that the decrease in center intensity and consequent increase in the intensity of the outer parts of the pattern will degrade the resolution of the lens. Proper choice of a focal point for the image plane will reduce the effect of aberrations on the diffraction pattern but even the selection of a "best" focal point will not eliminate the effect entirely.

If the wavefront aberrations are defined as the acoustical path length

$$W \equiv \overline{RP'}$$

with the sign of W taken as positive when the wavefront lies in front of the reference sphere BR, the effects of the choice of point O' can be investigated. Here, for simplicity, O' is chosen on the axis; however, this need not be the case. All that is required is that OO' define a ray which maintains its space orientation from object to image space even though the ray is refracted in the lens space.

Provided that the angle MRO' is not too large, an increase in the radius of the reference sphere simply adds a constant to W. However, if the center O' is moved to Q, as shown in Figure 5, the reference sphere more nearly "fits" the wavefront.

Let

$$W_o = \overline{RP'}$$

$$W_q = \overline{R'P'}$$

Then,

$$W_l \cong W_q - W_o = -\overline{RR'} \qquad (14)$$

is the change in aberration due to the longitudinal focal shift $\delta_z = O'-Q$. For δ_z small compared to $\overline{RO'}$ the following relation can be written

$$\overline{RA} = \overline{RO'} - \overline{O'Q}\cos\varphi = R - \delta_z \cos\varphi .$$

Thus the radius of the new reference sphere is

$$\overline{R'Q} = \overline{BQ} = R - \delta_z$$

and

$$\overline{RR'} = \delta_z (1-\cos \varphi)$$

so that

$$\triangle W_l = -(1-\cos \varphi) \delta_z \qquad (15)$$

Similar calculations yield

$$\triangle W_r = \sin \varphi \cos \gamma \delta_y \qquad (16)$$

where the variables are evident from inspection of Figure 6.

Equations (15) and (16) can be used to determine the "best" focus. Consider the aberration of a wavefront to be represented by the curve A in Figure 7. (For simplicity only longitudinal effects will be considered. Transverse effects can be computed in the same manner.)

Since the curve AA' is symmetric, the relation to equation (15) is all that one need consider [Ref. 8]. Plotting W vs $(1 - \cos \varphi)$ yields a pattern similar to that of Figure 8.

The horizontal distance between any straight line and the ordinate axis represents the change in W resulting from a longitudinal shift of the center of the reference sphere (combined with an appropriate change in the radius of the sphere). The focal shift as given by equation (15) is

$$\delta_z = \frac{1}{\text{slope (ST)}} \qquad (17)$$

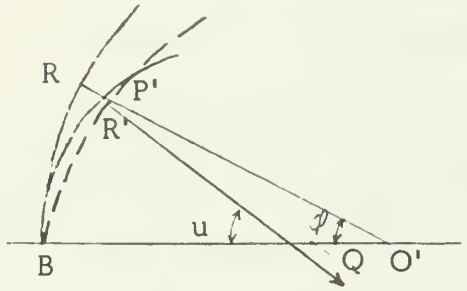

FIGURE 5

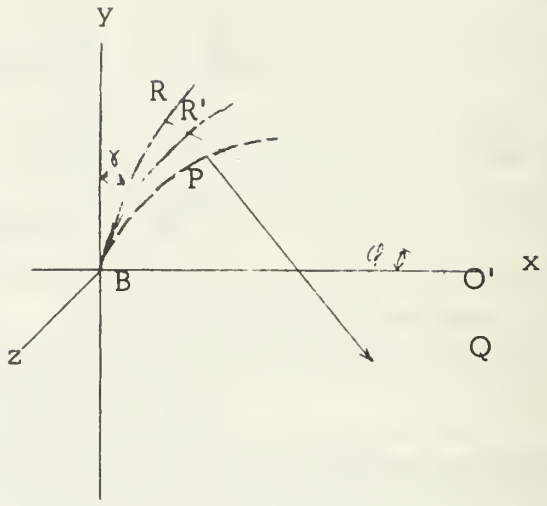

FIGURE 6

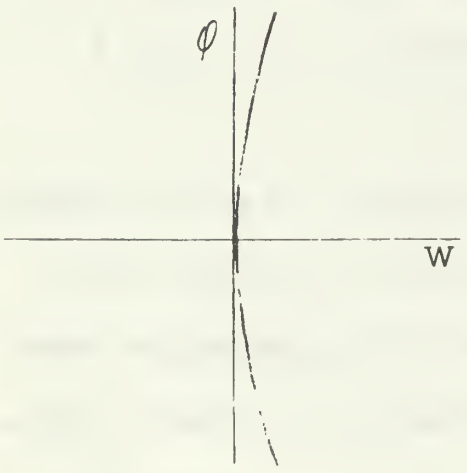

FIGURE 7

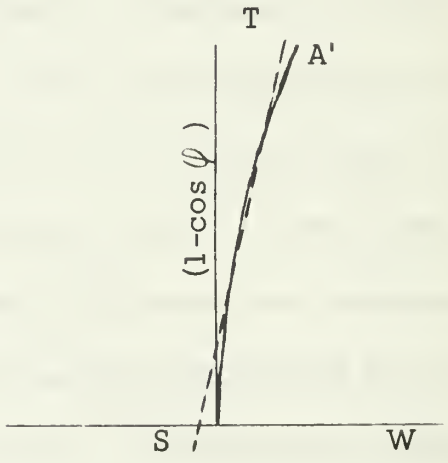

FIGURE 8

E. ADDITIONAL CONSIDERATIONS FOR AN ACTUAL LENS

In the construction of a real liquid lens the choice of material to constrain the refracting fluid in the desired physical shape is an important factor in the efficiency of the lens. In order to withstand the hydrostatic pressure required to form the lens, a strong, thin material with as good a ρc match to water as possible was desired. The only suitable material available in sufficient width was 0.012-inch stainless steel sheets. (Lens construction details may be found in section III-A.) The refracting liquid was hydrostatically pressurized to 1.4 atmospheres (twenty psi) to obtain spherically shaped biconvex lens surfaces and to overcome the effect of the liquid weight.

Since stainless steel has a value of ρc approximately twenty times that of water, the partial reflections due to the lens shell material are quite significant. Interference between the partial reflections from the front and back surface of the lens can manifest itself in at least two ways: A Fresnel zone plate effect, and a lengthening of the acoustic path due to multiple reflections within the lens. Both of these interference effects can produce multiple focal points.

1. Fresnel Zones - Newton's Rings

Consider a small cross section of the lens near the axis as shown in Figure 9.

The overall transmission coefficient for a wave at normal incidence can be computed by considering the problem in the same

manner as a transmission line [Ref. 11]. That is, find the impedance reflected to point A by the entire system and then calculate the

$$\text{reflection coefficient} = \overset{*}{P} = \frac{\overset{*}{Z}_a - Z_w}{\overset{*}{Z}_a + Z_w}$$

where $\overset{*}{Z}_a$ = the impedance reflected to point A

Z_w = the impedance of water

$$\text{transmission coefficient} = \overset{*}{T} = 1 + \overset{*}{P}$$

or

$$\overset{*}{T} = \frac{2\,\overset{*}{Z}_a}{\overset{*}{Z}_a + Z_w} \tag{18}$$

which is the pressure transmission coefficient for a wave normally incident upon the lens face. (Here, the asterisk above the symbol indicates a complex quantity.) The only additional assumption used here in the formulation of the theoretical effect of using a thin solid sheet to contain the refracting fluid is that the distance between the "parallel" surfaces decreases with increasing distance from the lens axis.

The pressure transfer coefficient for oblique incidence between two thick media is given more accurately by

$$\overset{*}{T} = \frac{2\,\overset{*}{Z}_a}{\overset{*}{Z}_a + R\,Z_w} \tag{19}$$

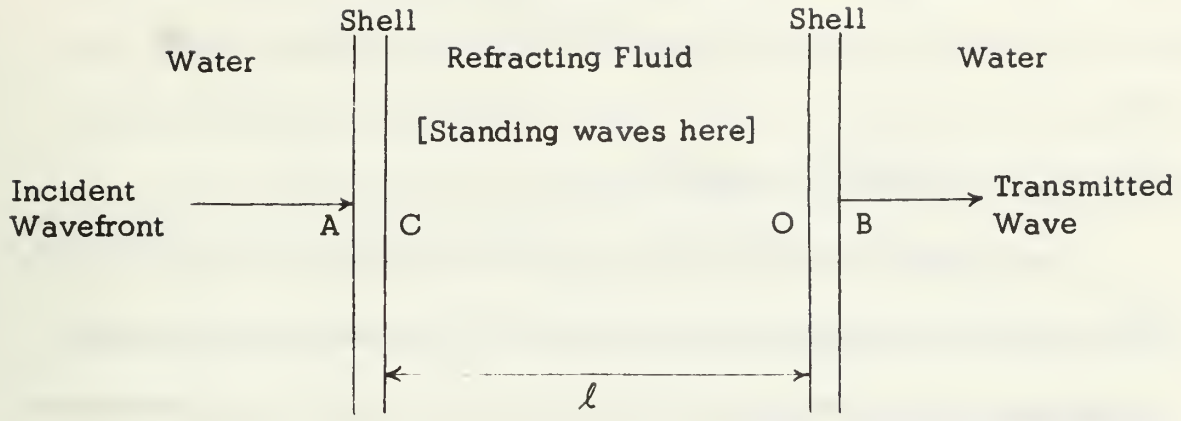

FIGURE 9

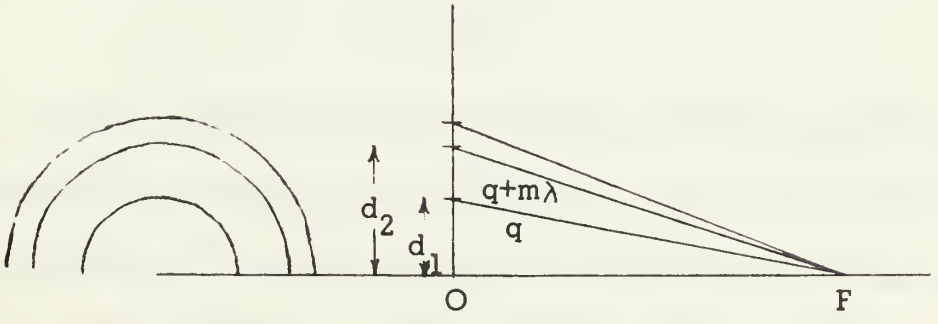

FIGURE 10

where

$$\overset{*}{R} = \left[\frac{1 - \left(\frac{C_e}{C_w}\right)^2 \sin^2 \theta_i}{1 - \sin^2 \theta_i} \right]^{1/2}$$

with

θ_i = angle of incidence of ray

C_e = speed of sound in the equivalent medium with impedance $\overset{*}{Z}_a$.

However, the transmission of sound through thin plates is a very complicated phenomenon [Refs. 9 and 15] and no significant improvement in accuracy is to be expected from using the thick-material formulas.

If the lens surfaces have large radii of curvature compared to the diameter of the lens, then as a first approximation the surfaces might be considered parallel for paraxial incident waves. This assumption is made in order to simplify the numerical calculations; however, the effect on the transmission coefficient resulting from the variation of distance between the lens surfaces cannot be neglected. (In fact, the quasi-parallel assumption was found to be erroneous for the conditions of the experiment. Nevertheless, its implications are explored in this section.)

Figure 18 is a plot of energy transmission coefficient,

$$T_e = 1 - \left| \overset{*}{P} \right|^2, \tag{20}$$

versus distance across the face of a lens such as that which has been described in the preceding paragraphs. It should be noted that there are regions (circular areas on the face of the lens) where nearly perfect

transmission occurs and there are other regions where negligible (less than fifty percent) transmission takes place. These alternate "dark" and "light" circles are similar to the opaque and transparent rings of the Fresnel zone plate or Newton's rings.

If the width of the "transmission zones" is narrow at the frequency of interest, then the point of maximum transmission coefficient (neglecting aberrations) can be considered as representative of a single wave through a zone. Figure 10 shows the geometry of the problem.

In order that the rays focus at point F

$$q^2 - d_1^2 = (q + m\lambda)^2 - d_2^2$$

or

$$q = \frac{d_2^2 - d_1^2 - m^2\lambda^2}{2m} \tag{21}$$

where d_i is the distance from the center of the lens to the ith point of maximum signal transfer.

Therefore, the described lens should focus incident acoustic waves at a point F where

$$\overline{OF} = (q^2 - d_1^2)^{1/2} . \tag{22}$$

The lens, therefore, has two real foci, one due to ordinary refraction and one due to Fresnel diffraction. The Fresnel zone effect also produces a virtual focus on the object side which results in diverging waves on the image side in addition to the converging waves.

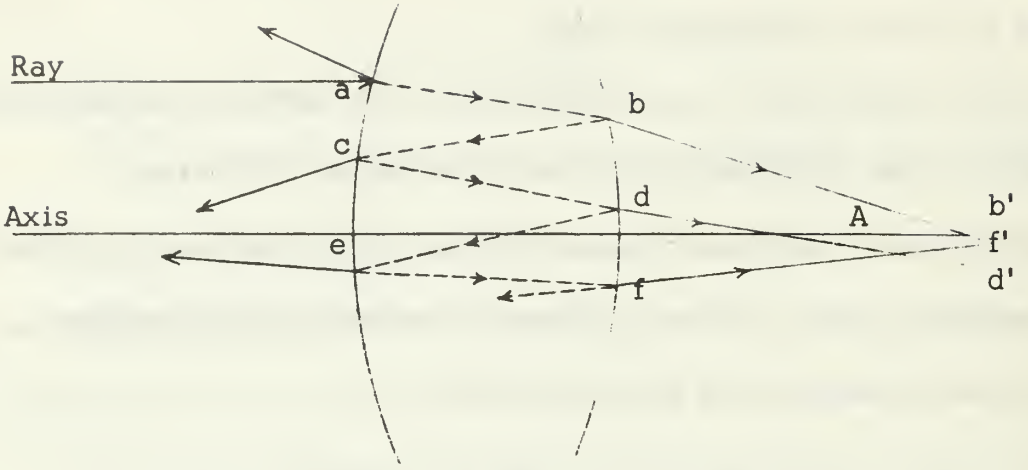

FIGURE 11

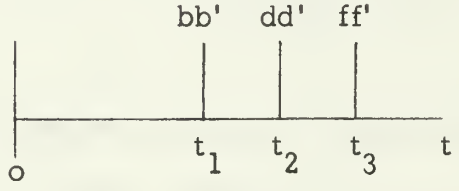

FIGURE 12

The results of computer modeling of this phenomenon are discussed in Section IV.

2. Multiple Reflections

If the surfaces are not quite parallel, which is the actual situation, then a ray will be reflected many times inside the lens. Figure 11 shows a possible path for one ray. As can be seen, each time the ray intersects a lens surface part of its energy is reflected and part is transmitted. That energy which is transmitted through the complete lens is not all focused at the same point, nor is it any longer in phase since each emerging ray travels a longer distance in the lens and each reflection is at a different angle.

In Figure 11 the angles are greatly exaggerated for clarity. However, for the problem under consideration the surfaces are only slightly curved and the rays bb', dd', and ff' would all pass near point A. Figure 12 is a time diagram showing the "time of arrival" of each ray at point A. The time between arrivals is approximately constant and should be about equal to two times the lens thickness divided by the velocity of sound in the refracting fluid.

In this case the lens has many foci corresponding to the multiply-reflected rays which exit the lens at the various radial distances from the axis. For a pulsed system (which is often used in practice because of reverberation effects) the time of arrival of the pulses can be correlated to time delays associated with an "average" thickness of the lens. The first pulse in time corresponds to the direct path; later pulses correspond to multiply-reflected paths.

III. EXPERIMENT

A. MECHANICAL DESIGN

The lens was designed so that $\frac{D}{\lambda}$ was approximately 200 at 400 KHz. (This requirement was dictated by the center frequency of the band-pass amplifiers used in a locally constructed underwater imaging system.) Therefore, a 76-cm (thirty inch) diameter lens was constructed. The pressure at the bottom of the lens when submerged was calculated to be

$$p_i = \rho_f gD - \rho_w gh' + \rho_w g(h'-D)$$

where

ρ_f and ρ_w are the densities of the fluid and of water, respectively

g is the acceleration due to gravity

D is the lens diameter (30 inches)

h' is the depth of the bottom of the lens under water

The depth of the lens below the water surface is limited by the anechoic tank to approximately six feet. The specific gravity of the refracting fluid is 1.47 as given in Section III-B. Thus we have for the lens under consideration

$$p_i = 0.47\, \rho_w gD$$

or the maximum internal pressure due entirely to the weight of the fluid is

$$p_i \approx 0.5 \text{ psi}$$

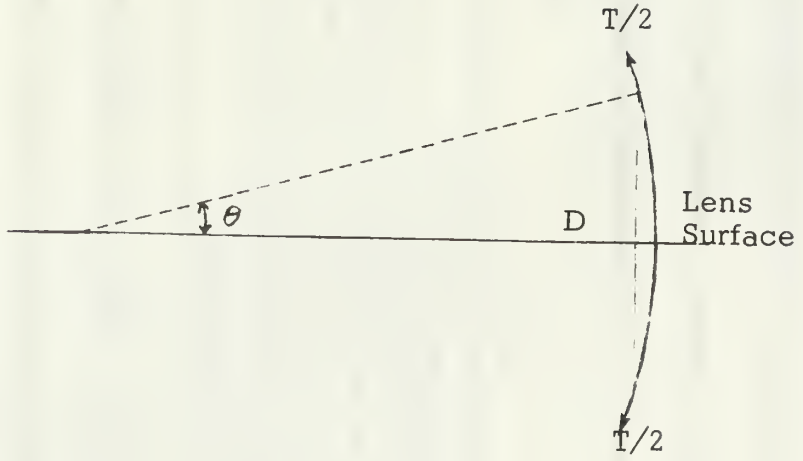

FIGURE 13

As an approximation, an internal hydrostatic pressure greater than twenty times the value calculated above, or 10 psi, should be enough to reduce the bulging effect of the refracting fluid weight to a negligible amount. However, the actual pressure used depends on the desired curvature of the lens surface and the mechanical properties of the lens face material.

If the radius of curvature of the lens face is two meters, then the force resulting from ten psi hydrostatic pressure is

$$F = PA = 7.2 \times 10^{3} \text{ lbs}$$

The "tension force" in the surface material is approximated by

$$T = \frac{F}{\sin \theta}$$

where θ is the angle shown in Figure 13.

Since the tension force as defined above effectively acts on the cross-sectional area of the entire circumference of the lens surface, the expected stress is approximately

$$\sigma = \frac{T}{\pi Dt} = \frac{F}{\pi Dt \sin \theta}$$

The assumptions as to internal pressure, radius of curvature of lens, and the diameter of the lens result in a thickness of

$$t = \frac{400}{\sigma} \text{ inches} \qquad (23)$$

The thinnest, readily available material which met the requirements of equation (23) was 0.012-inch stainless steel. The ultimate tensile stress of stainless steel is on the order of 160,000 psi; therefore,

a minimum thickness of about 0.0025 inch is required. Actually, the internal pressure is determined by the yield stress of the material. The yield strength of stainless steel is on the order of 100,000 psi so that stainless steel about 0.004 inch thick was desired.

Had Duraluminum (a heat-treated aluminum-copper alloy) sheets been available in the thickness of the stainless steel, the internal pressure could have been reduced in order not to exceed its ultimate tensile stress of 45,000 psi. Reducing the pressure increases the effect of the liquid weight; however, stainless steel was chosen for the lens material because it was available in large thin sheets and Duraluminum was not.

The stainless steel actually used was approximately three times thicker than the material desired. Severe acoustic reflections were expected but the focusing action of the biconvex lens and the feasibility of the mechanical design could still be demonstrated. Redesign with optimum material could be accomplished at a later time.

Figure 14 shows the assembly details of the lens that was constructed to provide experimental verification of the theory proposed in Section II. The lens base was constructed from 1-1/4 x 36 x 37-inch aluminum plate. A 1.5-inch flat seat was machined around the hole on each side of the plate and a groove for a one-quarter-inch O-ring was cut in each seat. Stainless steel sheets 0.012-inch thick were cut and punched as shown. The clamp rings were cut from one-quarter

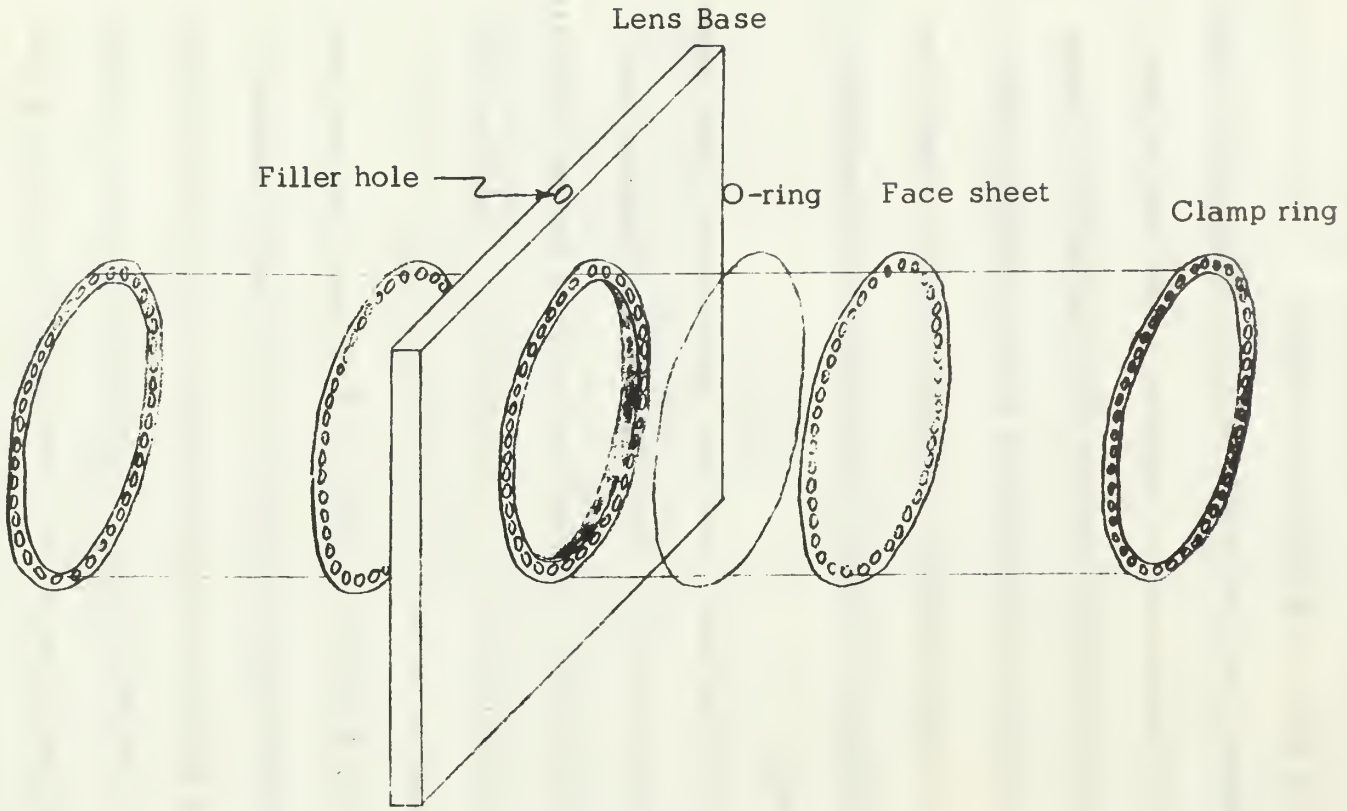

Lens Assembly

FIGURE 14

Front View

FIGURE 15a

Side View

FIGURE 15b

inch aluminum plate. Stainless steel bolts, 2.5 inches long, passing completely through the lens base on 2.8-inch center spacing held the finished components together. The lens was filled through the hole at the top and then hydrostatically pressurized to 1.4 atmospheres (twenty psi) with a hand operated hydraulic pump. Specially made Viton material O-rings were used in order to withstand the chemical action of the lens fluid.

Figure 15 shows front and side views of the experimental lens. The "scalloping" at the outer edge of the lens surface is discussed in Section III-F.

Figures 16 and 17 show the vertical and horizontal curvature across the faces of the lens with internal pressure at twenty psi. Measurements were made approximately five centimeters apart with a spherometer. It should be noted that the effect of liquid weight deformation is negligible as desired. However, the entire lens was now somewhat "biscuit shaped" due to failure of the clamp ring to completely restrain the face sheets. A large part of the tension was supported by the bolts through the holes in the sheets. This caused the outer edges to buckle and become scallop shaped. Increasing the number of clamping bolts minimized the buckling effect.

B. REFRACTING FLUID

Since the lens is so large, economy dictated that a low-priced refracting fluid be used. Accordingly, trichlorotrifluoroethane, a

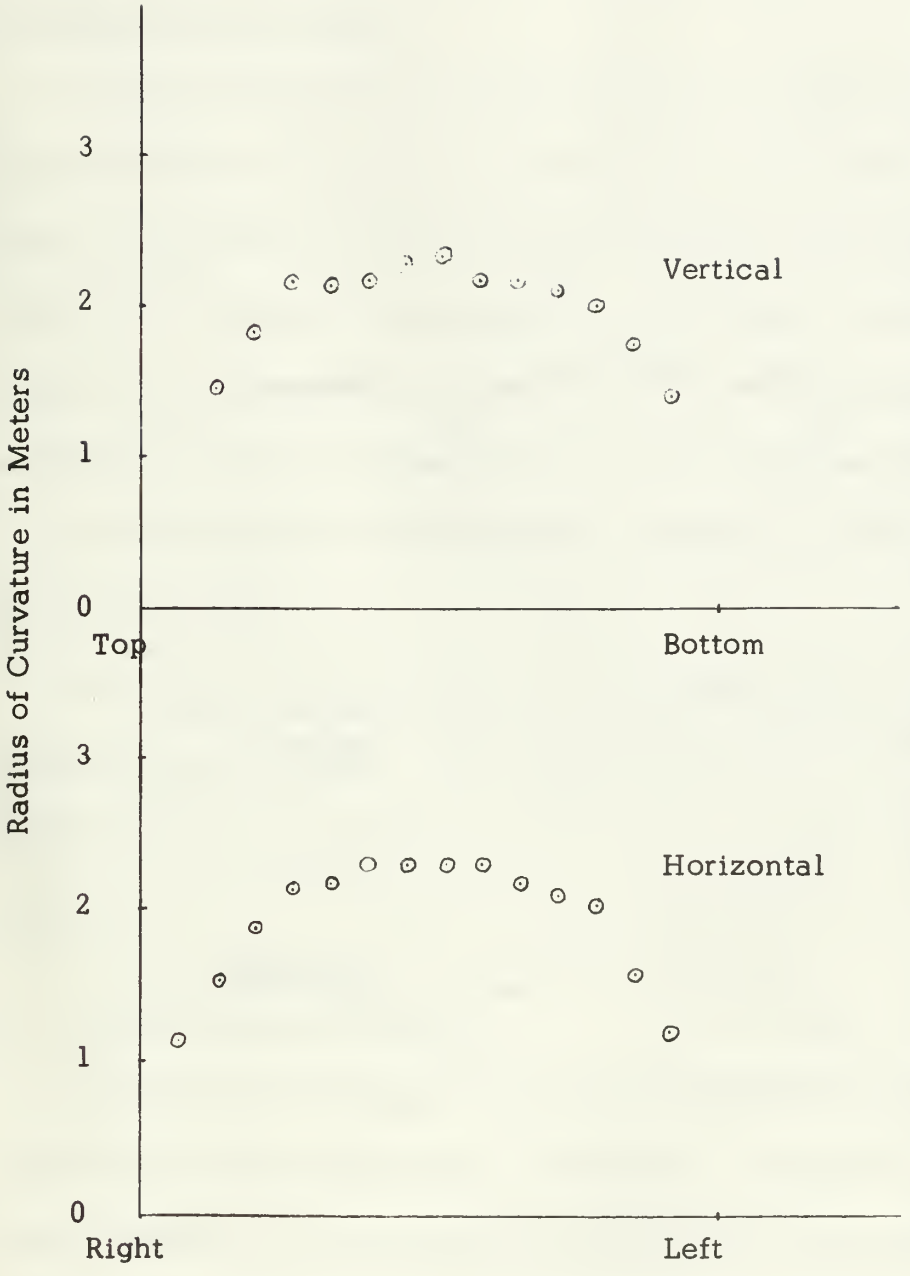

FRONT FACE

FIGURE 16

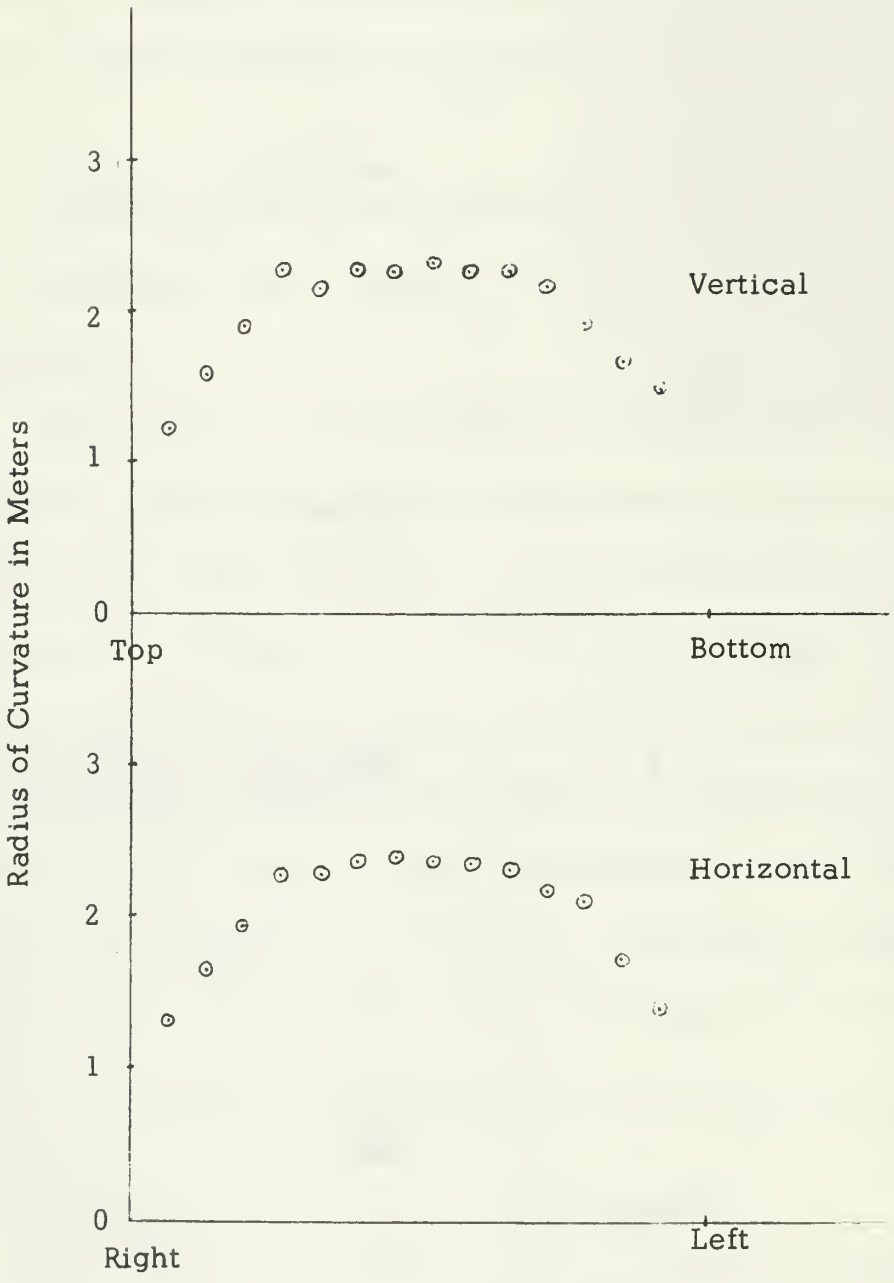

BACK FACE

FIGURE 17

commercial solvent (marketed under the name of Genesolve D) was purchased. Its sound velocity was determined relative to that of degassed distilled water at atmospheric pressure and a temperature of 26.5°C, and its density was measured.

Index of refraction was found to be 1.95 using the normal-mode resonance method in a fluid sphere (frequency of resonance in water = 7295.0 Hz; frequency of resonance (same mode) in Genesolve D = 3728.4 Hz). Because of imperfections in the container and the additional stress resulting from the greater density of the refracting fluid, it was impossible to use frequencies other than the fundamental mode. Therefore, no determination of the frequency dependence of the index of refraction was made.

The specific gravity of the fluid was determined by weighing equal volumes of fluid and water. The measured value was 1.47. Genesolve D, therefore, has an "impedance" (ρc) of 1.11×10^6 rayls compared to the value of 1.48×10^6 rayls for water given in Ref. 10.

C. COMPUTER SIMULATION

A computer program was developed to provide the calculations required by the theory developed in Section II. In general, the program traces individual unit-magnitude pressure "rays," of an incident plane wave in three dimensions, through the surfaces of the lens to the point where an individual "ray" lies on the surface of equal acoustic distance.

(Acoustic distance is referenced to an arbitrary surface which touches the lens surface at the point of tangency of the incoming wave.) The amplitude of each "ray" intersection is then modified by the complex transmission coefficient. Kirchoff's integral [Ref. 12] is then approximated by picking points in the image space and summing the complex amplitude at that point due to each "ray" traced. The method is similar to that used by Folds and Brown [Ref. 6] and Boyles [Ref. 4].

For point-source objects not at infinity (and off axis, if desired) a modified computer program was developed. The surface of constant phase is taken to be the surface where each ray acoustic distance is equal to the acoustic distance of the object ray which is directed toward the physical center of the lens. This limits the accuracy of off-axis computation. In addition, the minimum distance to the lens is limited by the critical angle of exit from the lens fluid, whereas the maximum distance is limited by the accuracy of the computer cosine sub-routine.

Figure 18 shows how the theoretical energy-transmission coefficient varies across the face of the lens when filled with water rather than lens fluid. The frequency of the incident wave is assumed to be 300 KHz. The left side corresponds to the center of the lens; the right side corresponds to the outer edge.

Measurement of the distances to the first maximum (d_1) and the second (d_2), etc., and utilization of equation (21) results in $m = 2, 4, 6, \ldots$ as a "best" solution for q = constant.

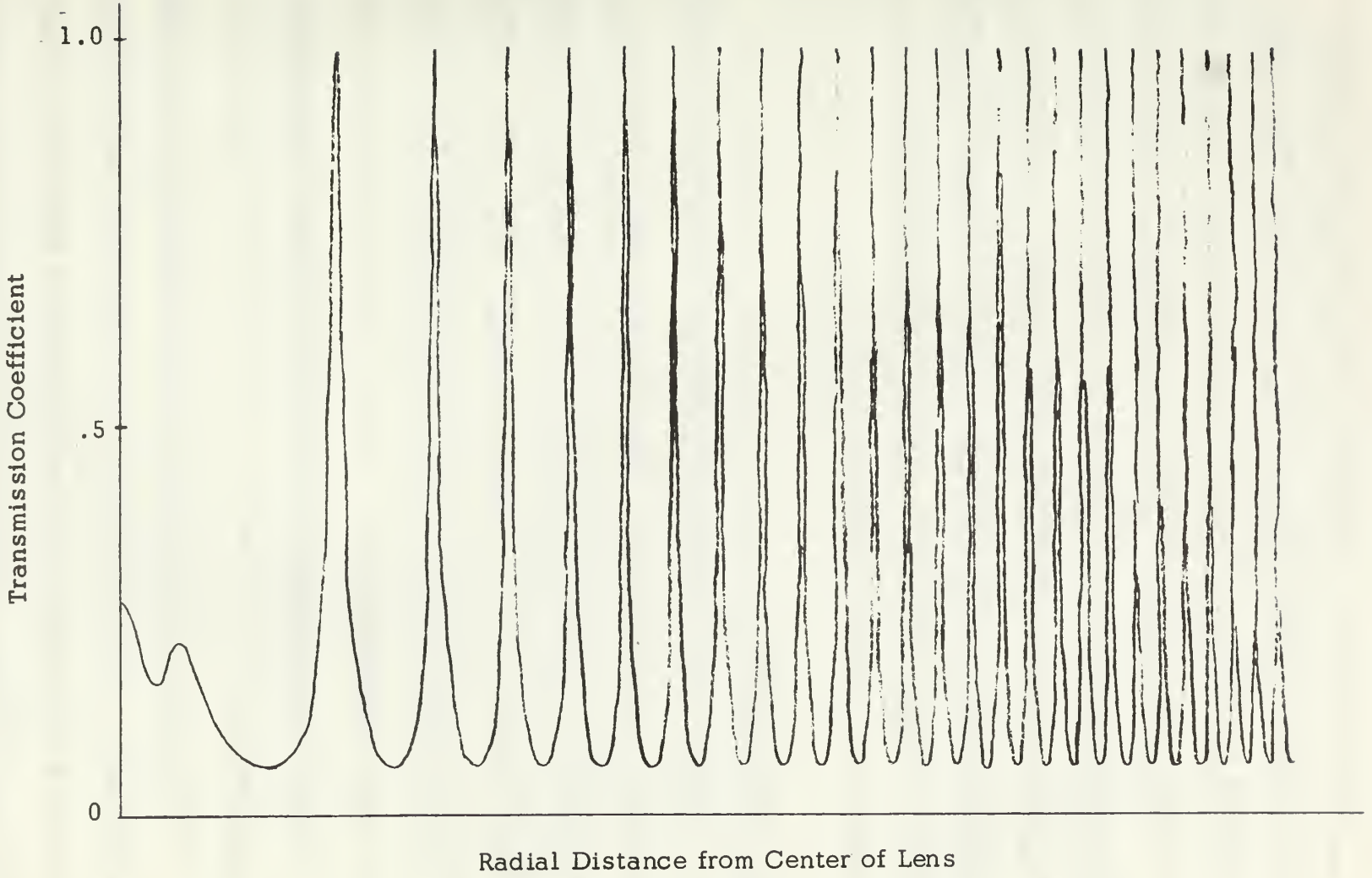
1.0
.5
0
Transmission Coefficient
Radial Distance from Center of Lens

FIGURE 18

These values for m correspond to the "best" value for frequencies from 100 KHz to 600 KHz when the fluid in the lens is water. Thus according to equation (22) the principal focal point of the water-filled lens at 300 KHz is estimated to be 22.5 centimeters. Similar calculations for a principal Fresnel focal point of the lens filled with Genesolve D and frequency of incident wave at 300 KHz yield 16.1 centimeters. The refractive focal point determined by geometric theory as calculated from equation (8) is 83 centimeters. Computed diffraction patterns are compared with measured patterns in Section IV.

D. TRANSDUCERS

One U.S. Navy standard E-8 transducer was used for the transmitter and a one-eighth-inch cylindrical barium titanate transducer was used as an omnidirectional receiver probe. A spun-aluminum parabolic mirror was used to develop a nearly plane wave at the surface of the lens. Figure 19 shows the general experimental set up.

E. TEST CONDITIONS

Tests were performed in the anechoic tanks at the Naval Postgraduate School.

A distance of 4 meters was maintained between the source object and the lens. Lens and transmitter were placed 1.45 meters below the surface. A pulse width of 0.1 milliseconds at a 1-KHz rate was used for all tests. Sound velocity in the tank was approximately 1465 m/sec.

Tests on a single sheet of the stainless steel used for the lens face indicate that the loss of signal through the plate in water is independent of the angle of incidence up to the measured angle of 16°. This loss was measured at 400 KHz to be 6.4 db which compares reasonably well to 7.1 db calculated by equation (17). This large loss is the result of using lens face material which is too thick and does not match the impedance of water. Stainless steel sheet 0.004-inches thick was desired but was not available in sufficient width.

F. PROBLEMS ENCOUNTERED

One problem which occurred as a result of the mechanical design was the scalloping of the outer edge of the lens when pressurized. The magnitude of scalloping was reduced by increasing the number of clamping bolts in the outer edge from 36 to 106; however, the effect was never eliminated. Scalloping was due to the fact that the shell material was much stronger than necessary, and the regions near the edges pulled away from the clamp bolts instead of just deforming due to the pressure. Results of the diffraction-pattern measurements are shown in Section IV for the full lens. However, a 30-cm-diameter aperture stop was placed in front of the center of the lens in order to provide the best experimental verification of the theory. This stop eliminated the effects of the scalloping and the sharper curvature of the outer regions of the lens since it blocked the signal except in the nearly constant-curvature center section of the lens.

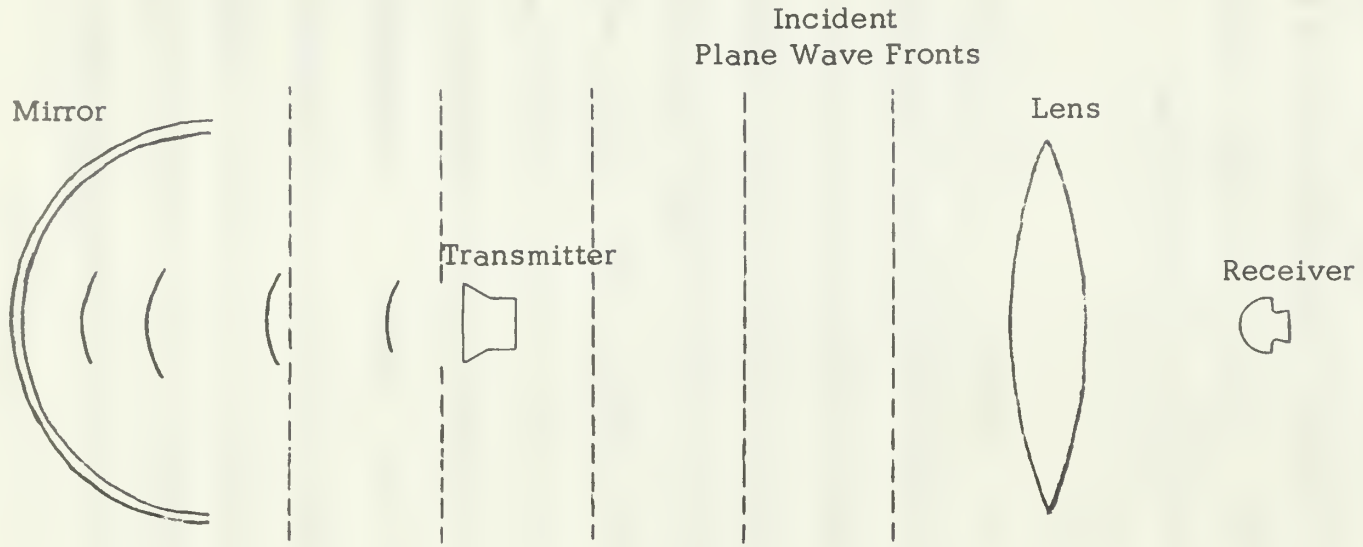
Incident
Plane Wave Fronts
Mirror
Transmitter
Lens
Receiver

FIGURE 19

Another incidental problem was corrosion of the aluminum lens base under the O-ring. An initial hydrostatic test of the lens was made using water. The water was then drained and the lens stood open (through the filling hole) for a week. The lens was then filled with Genesolve D and pressurized. Approximately three months later the lens began to lose fluid. Disassembly of the lens revealed corrosion under the O-rings which was probably due to the water residue left after the initial hydrostatic test. The grooves were cleaned and O-rings were replaced. No further leakage was noted.

IV. TEST RESULTS

Figure 20 shows the experimental diffraction pattern obtained from the wide-open lens at a frequency of 285 KHz. The amplitude scale is only relative. Actual intensity gain at the focal point relative to the signal level when the lens was out of the water was measured to be 20.4 db. Theoretical gain for this value of $\frac{D}{\lambda}$ is approximately 53 db. The low gain obtained experimentally is ascribed to reflection loss and aberrations.

The variation in radius of curvature across the lens surfaces was shown in Figures 16 and 17. The receiver was located at a "best" focal point which was 1.38 meters from the center of the lens. ("Best" focal point was determined as the axial point where maximum pressure occurred.) The pattern obtained was similar to that which was qualitatively expected. However, the focal point was about fifty centimeters beyond the value calculated in equation (8) and the center lobe beamwidth was approximately five times the beamwidth obtained from equation (10).

A thirty-centimeter-diameter stop was placed six centimeters in front of the lens in order to take advantage of the portion of the lens with the most constant radius of curvature. Figures 21, 22, and 23 show the comparison between the measured diffraction pattern and the computer (theoretical) diffraction pattern at three different frequencies.

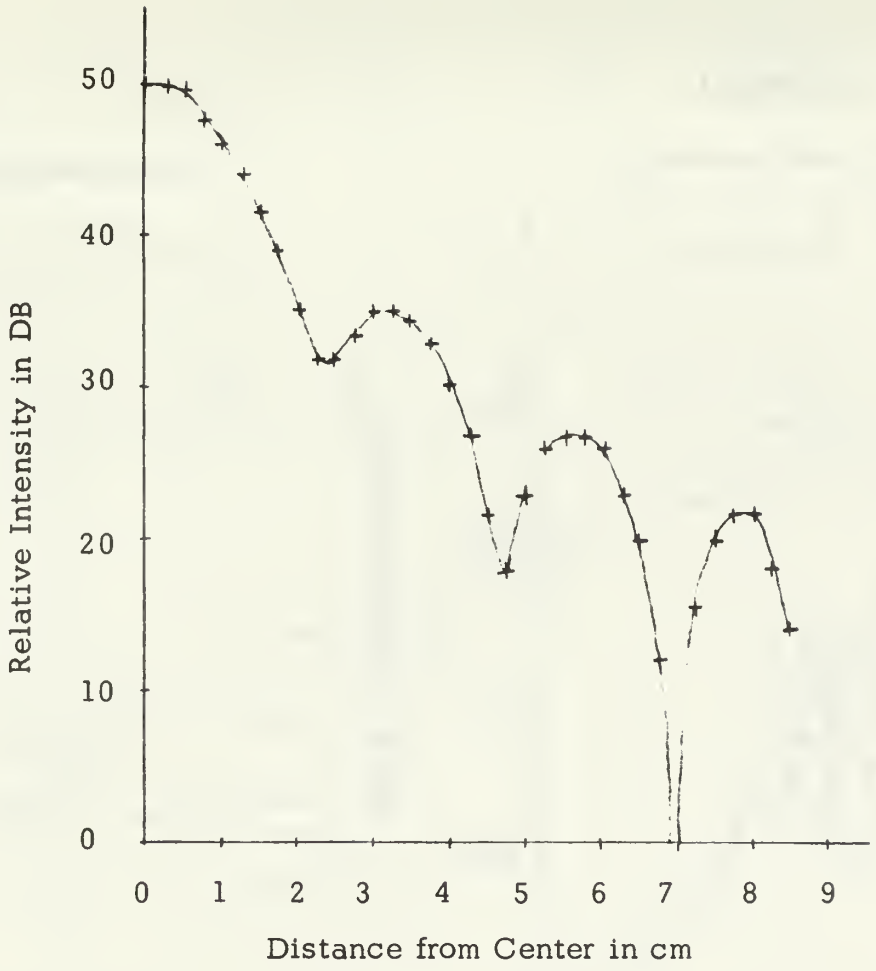
Relative Intensity in DB
50
40
30
20
10
0
0 1 2 3 4 5 6 7 8 9
Distance from Center in cm

FIGURE 20

FIGURE 21

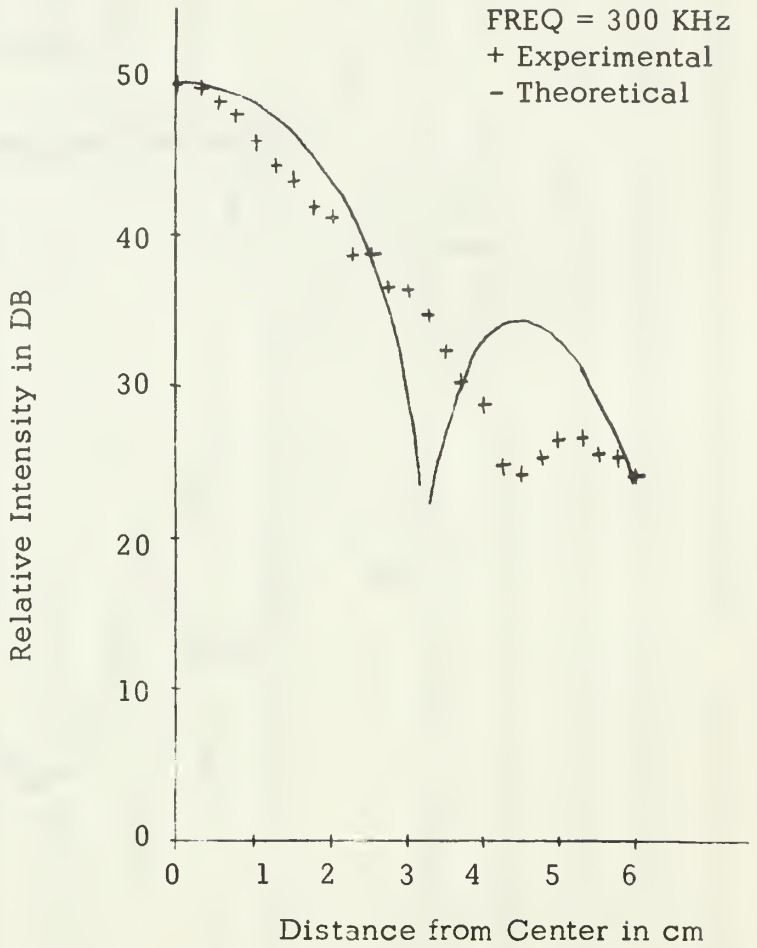

FIGURE 22

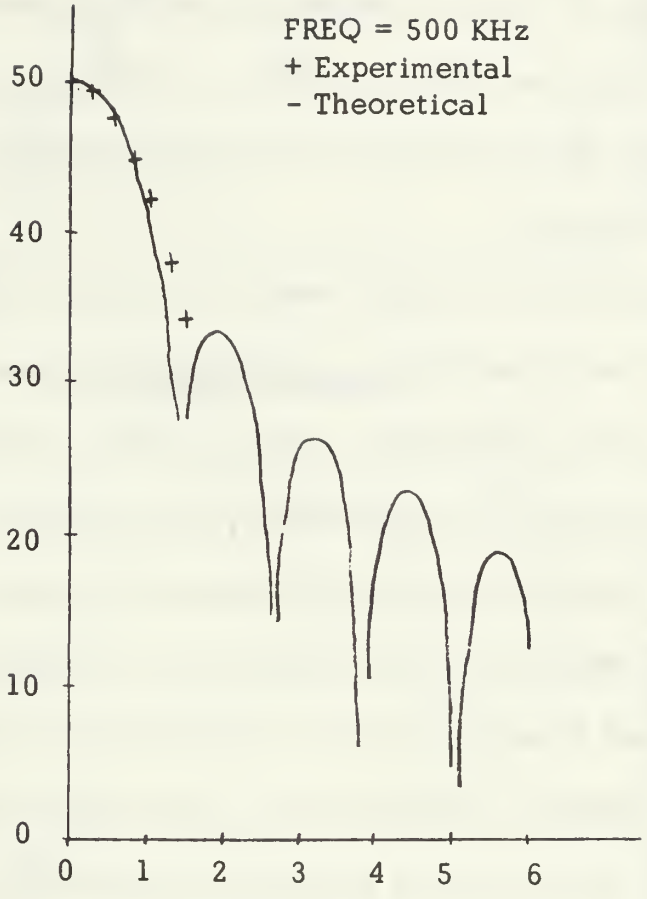
FREQ = 500 KHz
+ Experimental
- Theoretical
50
40
30
20
10
0
0
1
2
3
4
5
6

FIGURE 23

The intensity gain at the focal point relative to the signal level when the lens was out of the water was measured to be 4.7 db at 300 KHz. In this case the additional decrease in measured gain is attributed primarily to the reduced aperture.

For the case with the stop in position the computer solution for the focal point was 1.23 meters and the experimental value was 1.21 meters. The measured beamwidths are slightly larger than the computer calculated values and they are about three times the beamwidth obtained from equation (10).

Additional focal points were found at axial points closer to the lens. As mentioned before, a pulsed waveform was used in order to eliminate the reverberations in the test tank. As the receiver was moved toward the lens, additional pulses appeared on the oscilloscope monitor. Each new pulse that appeared did so later in time on the trace. The pulse which was used to measure the diffraction patterns of Figures 21, 22, and 23 was the "first" pulse received in time. The second pulse appeared at a measured time of 0.4 milliseconds after the first pulse and had a maximum amplitude 21 centimeters from the center of the lens (on the lens axis). A third and fourth pulse appeared as the receiver probe was moved closer to the lens, but neither of these pulses seemed to maximize before the receiver probe contacted the lens face.

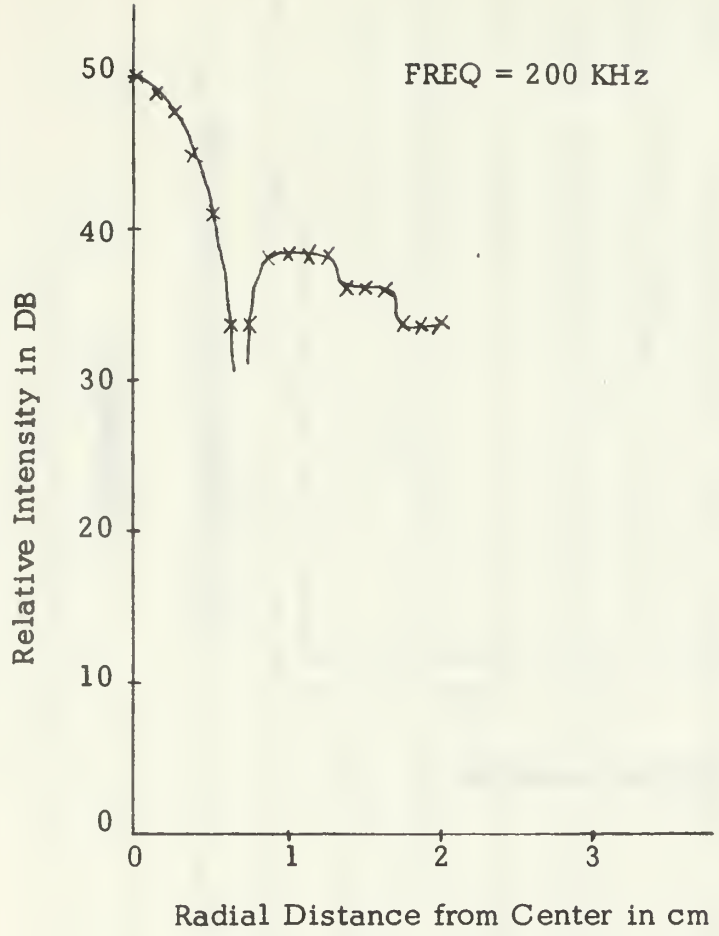

FIGURE 24

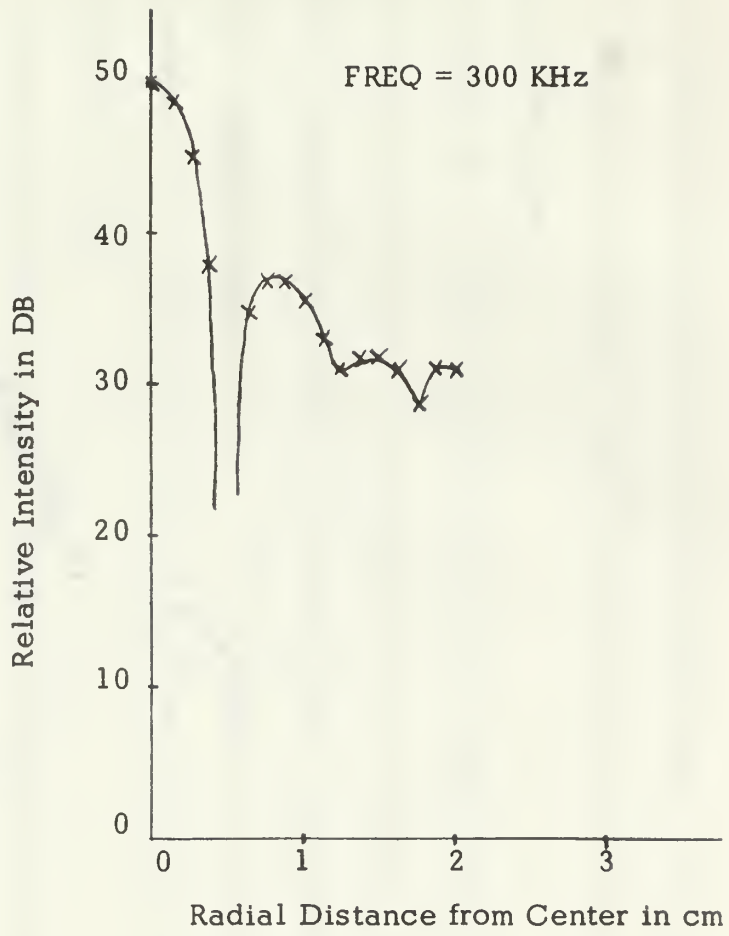

FIGURE 25

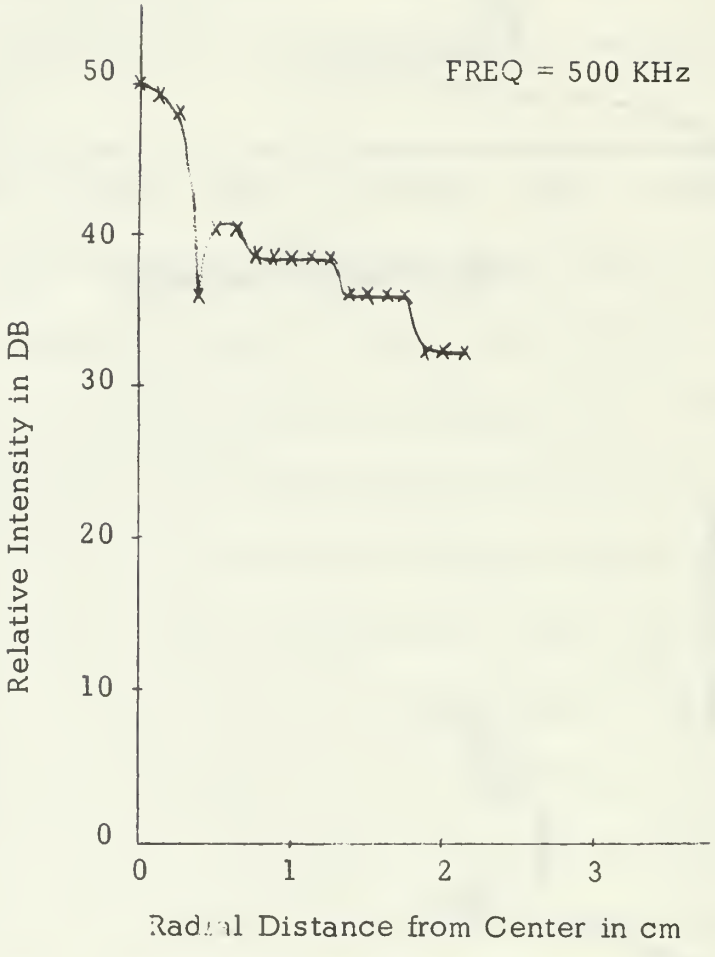
FREQ = 500 KHz
Relative Intensity in DB
50
40
30
20
10
0
0
1
2
3
Radial Distance from Center in cm

FIGURE 26

The third pulse trailed the second by about 0.4 milliseconds and the fourth pulse trailed the third by about 0.45 milliseconds. No evidences of Fresnel zones were observed when the probe was moved radially across the lens face.

Figures 24, 25, and 26 show the experimental diffraction patterns for the second pulse measured at 21 centimeters from the lens. At 300 KHz the measured beamwidth of the center lobe is nearly equal to the beamwidth obtained from equation (10). The intensity gain at this point, relative to the signal level when the lens was not in the water, was measured as 5 db.

Figure 27 shows the measured variation of beamwidth and sidelobe level versus frequency for the stopped-down lens with focal point at 1.21 meters. A theoretical curve based on the dimensions of the lens and equation (10) is included for comparison.

Figure 28 shows the same information as Figure 27 for the "focal point" at 21 centimeters. Due to the scatter of data the 1/f characteristic of the beamwidth is not as apparent as it is in Figure 27.

Data from off-axis source points was also obtained and additional aberrations for points up to 15° off-axis were found to be insignificant.

A final test of the lens mechanical design was performed by increasing the hydrostatic pressure in the lens. At 25 psi the radius of curvature was 1.92 meters and the constant-curvature portion had increased in diameter to approximately 35 centimeters. At a pressure of thirty psi the radius of curvature was 1.73 meters and the constant-

curvature portion was still 35 centimeters in diameter. The experimental focal point had shifted from 1.21 to 1.09 meters. Forty psi was the maximum pressure obtained. At this value of internal pressure the radius of curvature was 1.37 meters and the constant-curvature portion had increased to about 50 centimeters. The focal point had decreased to 0.98 meters. Approximately thirty minutes after the lens had been pressurized to forty psi the back lens face began to pull away from the clamp ring and the bottom portion became quite distorted and scalloped.

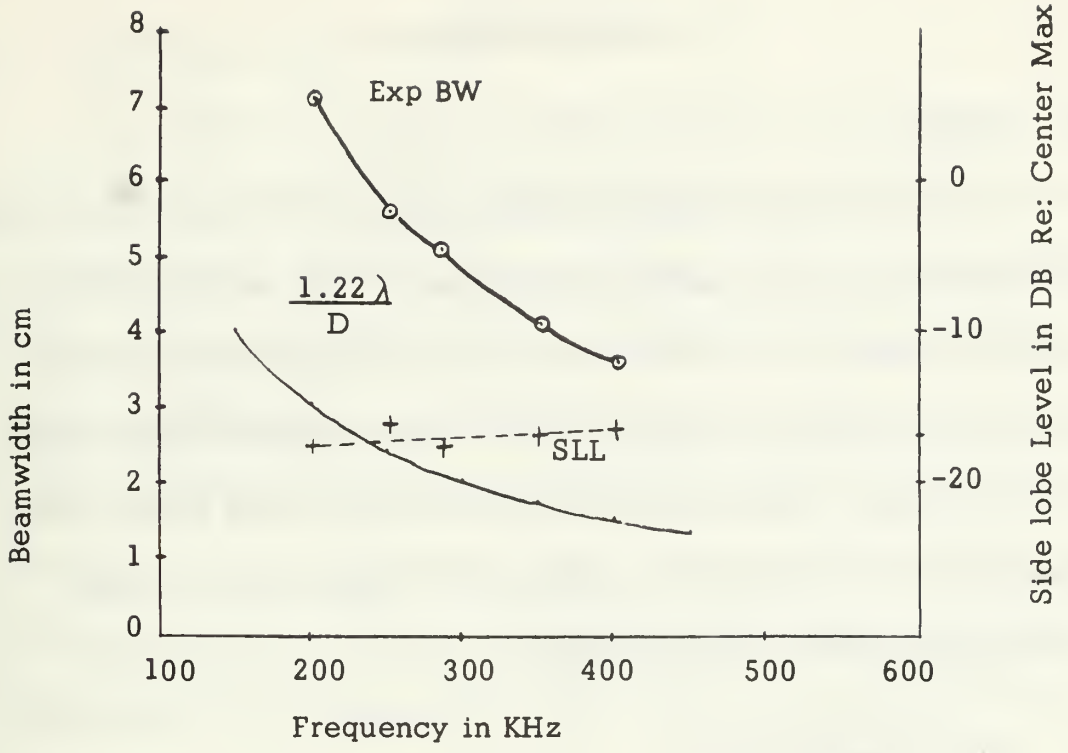

FIGURE 27

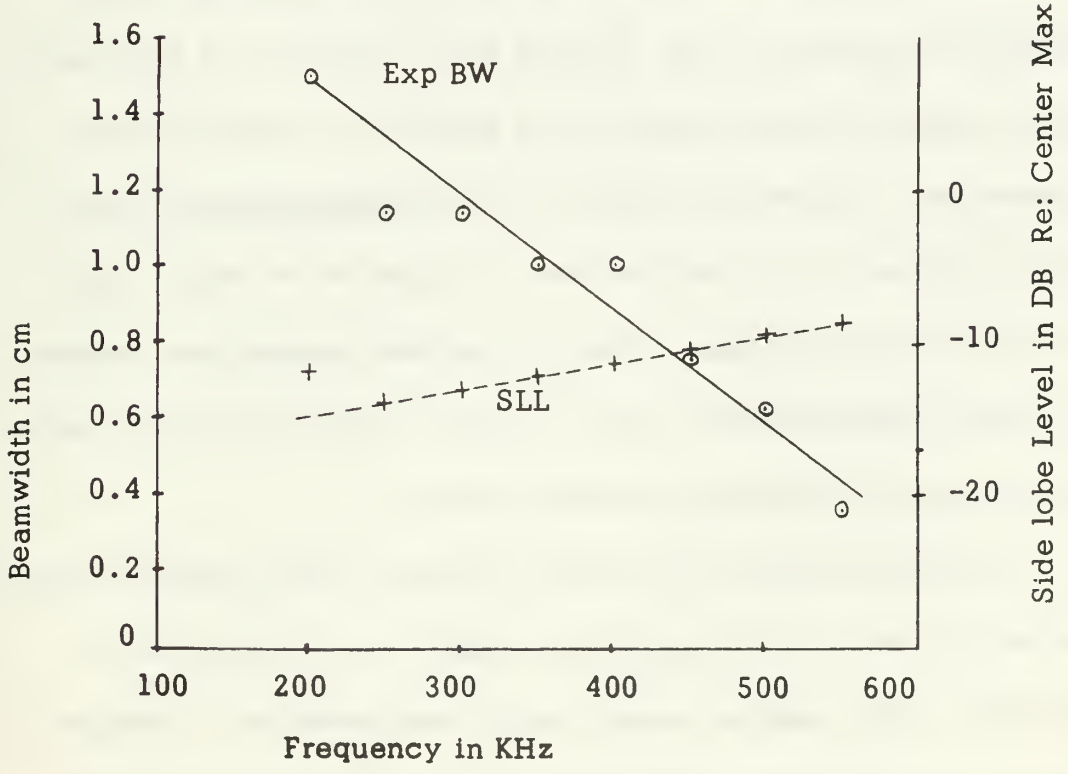

FIGURE 28

V. CONCLUSIONS

A. GENERAL

It has been shown that qualitative results for a liquid-filled lens can be predicted from relatively simple theory. The experimental data verifies the fact that a biconvex liquid lens does focus the acoustic energy with a diffraction pattern close to that calculated numerically. For the lens used in this experiment the beamwidths and losses were larger than desired but use of thinner and/or less dense lens face material should reduce these effects.

B. LENS CONSTRUCTION

Since each sheet of metal has slightly different mechanical properties even within itself, the lens face curvature as a function of internal pressure cannot be accurately predicted. In addition, Ref. 17 indicates that a spherical surface can only be approximated by the elastic deformation of a circular plate, clamped at the edge, under a constant force per unit area. Thus for maximum useable lens surface an internal pressure which creates a stress in the lens surface greater than the material yield stress must be used.

As demonstrated by the surface distortion after a short time under a pressure of forty psi, the lens face material must not be free to move even a slight amount radially when under pressure. A thicker clamp ring with perhaps a step and mating flange should eliminate this problem.

C. MULTIPLE FOCAL POINTS

As expected, more than one focal point was found. However, these points were associated with pulses which arrived at the receiver probe at different times. Since the measured times of arrival compare closely with the time required for a wave to travel through multiples of two thicknesses (24 centimeters) inside the lens, it is concluded that multiple reflections inside the lens and not a Fresnel zone effect are responsible for the multiple focal points. Furthermore, no Fresnel zones of transmission were observed near the lens face. Apparently partial reflections do not interfere sufficiently to produce a significant "Newton's rings" effect.

LIST OF REFERENCES

1. Boyles, C. A., "Theory of Focusing Plane Waves by Spherical, Liquid Lenses," The Journal of the Acoustical Society of America, v. 38, p. 393-405, September 1965.

2. Boyles, C. A., "Wave Theory on an Acoustic Luneberg Lens," The Journal of the Acoustical Society of America, v. 43, p. 709-715, April 1968.

3. Boyles, C. A., "Radiation Characteristics of Spherically Symmetric, Perfect Focusing Acoustic Lenses," The Journal of the Acoustical Society of America, v. 45, p. 351-355, February 1969.

4. Boyles, C. A., "Wave Theory of an Acoustic Luneberg Lens. II. The Theory of Variable Density Lenses," The Journal of the Acoustical Society of America, v. 45, p. 356-364, February 1969.

5. Folds, D. L. and Brown, D. H., "Focusing Properties of Cylindrical Liquid-Filled Acoustic Lenses with Large Diameter-to-Wavelength Ratios," The Journal of the Acoustical Society of America, v. 43, p. 560-565, March 1968.

6. Folds, D. L. and Brown, D. H., "Comments on Focusing Properties of Cylindrical Liquid-Filled Acoustic Lenses with Large Diameter-to-Wavelength Ratios," Eby, E. S., Fein, M. O., and Burt, P. J.: and reply thereto, The Journal of the Acoustical Society of America, v. 44, p. 1744-1745, December 1968.

7. Foss, R. N. and Levine, S., "An Underwater Imaging System," p. 77-99, Ultrasonic Imaging and Pulse Gated Light, Proceedings of a Symposium, Mine Advisory Committee, December 1965. CONFIDENTIAL.

8. Hopkins, H. H., Wave Theory of Aberrations, p. 1-34, Oxford University Press, 1950.

9. Hueter, T. F. and Bolt, R. H., Sonics, p. 260-263, Wiley, 1965.

10. Jenkins, F. A. and White, H. E., Fundamentals of Optics, 3rd ed., McGraw-Hill, 1957.

11. Kinsler, L. E. and Frey, A. R., Fundamentals of Acoustics, 2nd ed., Wiley, 1962.

12. Kraus, J. D., Electromagnetics, McGraw-Hill, 1953.

13. Longhurst, R. S., Geometrical and Physical Optics, Longmans, Green and Co., 1957.

14. Lord, G. E., "Acoustic Field in a Luneberg Lens," The Journal of the Acoustical Society of America, v. 43, p. 382-383, February 1968.

15. Mason, W. P., Physical Acoustics and the Properties of Solids, Van Nostrand, 1958.

16. Sears, F. W., Optics, 3rd ed., Addison-Wesley, 1958.

17. Timoshenko, S. and Woinowsky-Krieger, S., "Theory of Plates and Shells, 2nd ed., McGraw-Hill, 1959.

18. Toulis, W. J., "Acoustic Focusing with Spherical Structures," The Journal of the Acoustical Society of America, v. 35, p. 286-292, March 1963.

INITIAL DISTRIBUTION LIST

		No. Copies
1.	Defense Documentation Center Cameron Station Alexandria, Virginia 22314	20
2.	Library, Code 0212 Naval Postgraduate School Monterey, California 93940	2
3.	Ordnance Systems Command Department of the Navy Washington, D. C. 20360	1
4.	Assoc. Professor G. L. Sackman, Code 52Sa Department of Electrical Engineering Naval Postgraduate School Monterey, California 93940	5
5.	LCDR Jack L. Roudebush, USN R.R. #1 Crawfordsville, Indiana 47933	1
6.	Mr. D. L. Folds, Code 722 Navy Mine Defense Laboratory Panama City, Florida 32401	1

Security Classification

DOCUMENT CONTROL DATA - R & D

(Security classification of title, body of abstract and indexing annotation must be entered when the overall report is classified)

1. ORIGINATING ACTIVITY (Corporate author)	2a. REPORT SECURITY CLASSIFICATION
Naval Postgraduate School Monterey, California 93940	Unclassified
	2b. GROUP

3. REPORT TITLE

An Experimental Biconvex Liquid-filled Acoustic Lens

4. DESCRIPTIVE NOTES (Type of report and inclusive dates)

Electrical Engineer Thesis; June 1969

5. AUTHOR(S) (First name, middle initial, last name)

Jackie Lee Roudebush

6. REPORT DATE	7a. TOTAL NO. OF PAGES	7b. NO. OF REFS
June 1969	56	18

8a. CONTRACT OR GRANT NO.	9a. ORIGINATOR'S REPORT NUMBER(S)
b. PROJECT NO.	
c.	9b. OTHER REPORT NO(S) (Any other numbers that may be assigned this report)
d.	

10. DISTRIBUTION STATEMENT

Distribution of this document is unlimited.

11. SUPPLEMENTARY NOTES	12. SPONSORING MILITARY ACTIVITY
	Naval Postgraduate School Monterey, California 93940

13. ABSTRACT

An experimental study has been made of the properties of a biconvex liquid-filled acoustic lens formed by pressurizing a refracting fluid between two deformable diaphragms. Trichlorotrifluoroethane was used as the refracting liquid and stainless steel sheets 76 cm in diameter and 0.3 mm (0.012 inch) thick were used as the diaphragm material. Distortion of the spherical surfaces due to the weight of the liquid was negligible because of the tension developed by the internal hydrostatic pressure (1.4 atmospheres for focal length 1.2 meters). Acoustic diffraction patterns measured at f/4.0 in water at frequencies from 200 KHz to 500 KHz compare favorably with patterns computed numerically. Multiple focal points were found and can be associated with multiple internal reflections.

DD FORM 1 NOV 65 1473 (PAGE 1)

S/N 0101-807-6811

Security Classification

A-31408

14 KEY WORDS	LINK A		LINK B		LINK C	
	ROLE	WT	ROLE	WT	ROLE	WT
Acoustic lens						
Liquid-filled acoustic lens						
Biconvex acoustic lens						